



Solution-processed red iridium complexes based on carbazole-phenylquinoline main ligand: Synthesis, properties and their applications in phosphorescent organic light-emitting diodes

Myungkwan Song^a, Jin Su Park^a, Mikyoung Yoon^a, Ae Jin Kim^a, Young Inn Kim^a, Yeong-Soon Gal^b, Jae Wook Lee^{c,*}, Sung-Ho Jin^{a,*}

^a Department of Chemistry Education, Interdisciplinary Program of Advanced Information and Display Materials and Center for Plastic Information System, Pusan National University, Busan 609-735, Republic of Korea

^b Polymer Chemistry Lab., Kyungil University, Hayang 712-701, Republic of Korea

^c Department of Chemistry, Dong-A University, Busan 604-714, Republic of Korea

ARTICLE INFO

Article history:

Received 15 September 2010
Received in revised form
11 November 2010
Accepted 12 November 2010

Keywords:

Solution-process
PhOLEDs
Phosphorescent
Red
Hole transporting material

ABSTRACT

New carbazole-phenylquinoline (CVz-PhQ) based iridium complexes were designed and synthesized for their application in red phosphorescence organic light-emitting diodes (PhOLEDs) and their photophysical, electrochemical and electroluminescence (EL) properties were investigated. The PhOLEDs were fabricated using *bis*[9-(2-(2-methoxyethoxy)ethyl)-3-(4-phenylquinolin-2-yl)-9H-carbazolato-*N,C2'*]iridium 2-pyrazinecarboxylic acid (EO-CVz-PhQ)₂Ir(prz) and *bis*[9-(2-(2-methoxyethoxy)ethyl)-3-(4-phenylquinolin-2-yl)-9H-carbazolato-*N,C2'*]iridium 5-methyl-2-pyrazinecarboxylic acid (EO-CVz-PhQ)₂Ir(mprz) as the emitter and PVK, co-doped with OXD-7 as the electron transport material and TPD as the hole transport material, as the polymer host. The red emissive PhOLEDs, based on the ITO/poly(3,4-ethylenedioxythiophene):poly(styrenesulfonate) (PEDOT:PSS)/4,4',4''-tris(carbazole-9-yl)triphenylamine (TCTA)/poly(*N*-vinylcarbazole) (PVK):*N,N'*-diphenyl-*N,N'*-(*bis*(3-methylphenyl)-[1,1-biphenyl]-4,4'-diamine (TPD)):1,3-*bis*[5-(4-*tert*-butylphenyl)-1,3,4-oxadiazole-2-yl]benzene (OXD-7):Ir complex/cathode configuration, exhibited a maximum external quantum efficiency of 3.68% and a maximum luminance efficiency of 6.69 cd/A. Furthermore, by introducing a TCTA interlayer, the PhOLEDs showed only a slight efficiency roll off of 5.4% from a low current density (1.81 mA/cm²) to a high current density (44.59 mA/cm²).

Crown Copyright © 2010 Published by Elsevier B.V. All rights reserved.

1. Introduction

Organic light-emitting diodes (OLEDs) have been the subject of intense research in the past decade, because of their potential applications for large area flat panel displays and solid state lighting sources. Recently, OLEDs using phosphorescent materials such as iridium or platinum complexes as the emitting materials were reported, which showed a much higher efficiency than those using fluorescent emitting materials [1–3]. In particular, phosphorescent OLED (PhOLED) materials offer the possibility of developing highly efficient OLEDs, since they are able to achieve emission from both the singlet and triplet excited states. Therefore, an internal quantum

efficiency of up to 100% is theoretically possible. Many PhOLEDs have been fabricated by simultaneous or sequential vapor deposition of several organic layers [4,5], making the fabrication process relatively complicated and expensive, especially if large substrates are used. However, solution based manufacturing processes, such as spin coating and inkjet printing, provide an attractive alternative to vacuum deposition for the preparation of OLEDs, mainly due to their significantly reduced production cost. Therefore, it is desirable to investigate approaches to solution processable phosphorescent materials. Some of the research groups have been tried, including doping polymer host systems with phosphorescent materials and the synthesis of soluble phosphorescent complexes [6–8]. The reported quantum efficiencies were high, but were measured in an integrating sphere, and include both light emission from forward direction and waveguided light, thus are not directly compared to other device performances. The majority of OLEDs containing solution processed layers produced so far have contained oligomers

* Corresponding author. Tel.: +82 51 510 2727; fax: +82 51 581 2348.

** Corresponding author.

E-mail addresses: jlee@donga.ac.kr (J.W. Lee), shjin@pusan.ac.kr (S.-H. Jin).

or conjugated polymers [9–14] and the more recently fabricated ones contained dendrimers [15–20]. Phosphorescent polymers have been employed as solution processed emitting materials by chemically bonding iridium complexes in the side chain, main chain, or chain terminals [21–23]. Phosphorescent dendrimers are also employed, because of their inherent topological features [24], in which an iridium complex is surrounded by a branched shell to prevent the self-aggregation of the concentration quenching of the emissive core in the solid state. However, the performance of polymer- and dendrimer-based phosphorescent materials is significantly lower than that of their solution processable small molecule counterparts. Many attempts have been made to tailor the ligand structure in order to establish the relationship between the structures of the ligands and properties of the iridium complexes, and then develop good materials for red [25], green [26] and blue [27] OLEDs. It has been found that the emission wavelength of iridium complexes can usually be tuned by choosing appropriate substituents and changing their positions. For instance, the emission wavelengths of iridium complexes can be made to cover the entire visible region by modifying or varying the cyclometalated 2-arylpyridine main ligands and ancillary ligands [28]. Using this approach, we recently reported a novel red emitting iridium complexes based on carbazole (CVZ) containing phenylquinoline (PhQ) derivatives as an emitting layer for the fabrication of PhOLEDs by solution processing [29]. Therefore, in this paper, we report the synthesis, redox, photophysical, and electroluminescent (EL) properties of new red emitting heteroleptic iridium complexes containing pyrazine-based ancillary ligands for the solution processing of the emitting layer in the fabrication of PhOLEDs.

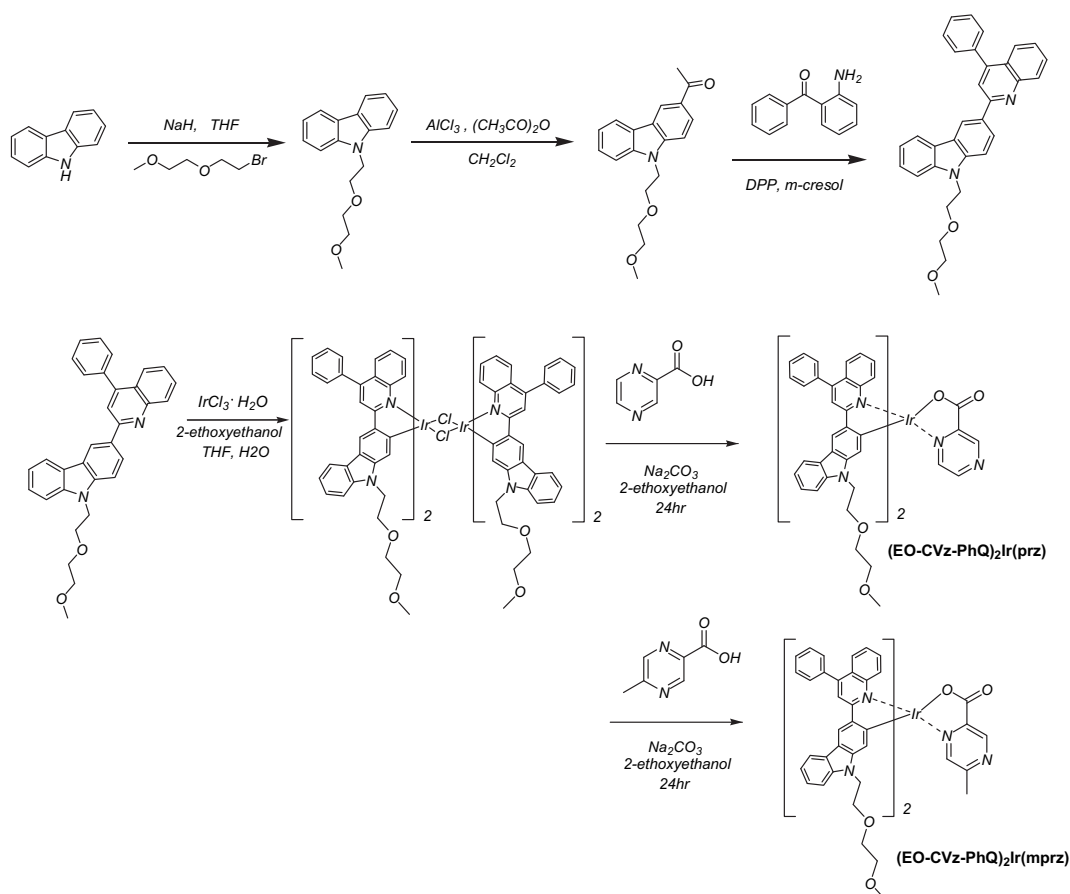
2. Results and discussion

2.1. Synthesis and characterization

Scheme 1 illustrates the synthetic procedures used for the preparation of (EO-CVz-PhQ)₂Ir(prz) and (EO-CVz-PhQ)₂Ir(mprz). The main ligand, 9-(2-(2-methoxyethoxy)ethyl)-3-(4-phenylquinolin-2-yl)-9H-carbazole (EO-PhQ-CVz) was prepared by an acid-catalyzed Friedlander condensation reaction. The reaction of 3-acetyl-N-2-(2-methoxyethoxy)ethylcarbazole with 2-aminobenzophenone resulted in the formation of the desired donor–acceptor type of CVz-PhQ with 80% yield. The cyclometalated iridium μ -chloride bridged dimer was synthesized from iridium trichloride hydrate with an excess of the main ligand using Nonoyama's method [30]. Two separate sodium carbonate-mediated ligand exchange reactions with 5-methyl-2-pyrazinecarboxylic (mprz) acid and 2-pyrazinecarboxylic acid (prz) ancillary ligands, respectively, were carried out to give heteroleptic iridium complexes in quantitative yield. These two iridium complexes were purified using silica column chromatography and recrystallization. The final products prior to device fabrication were characterized by ¹H and ¹³C NMR spectroscopy and elemental analysis.

2.2. Thermal properties

The thermal properties of the iridium complexes were examined by thermogravimetric analysis (TGA) and differential scanning calorimetry (DSC) under an N₂ atmosphere at a heating rate of 10 °C/min and their decomposition temperatures (T_d, corresponding to



Scheme 1. Synthetic routes for (EO-CVz-PhQ)₂Ir(prz) and (EO-CVz-PhQ)₂Ir(mprz).

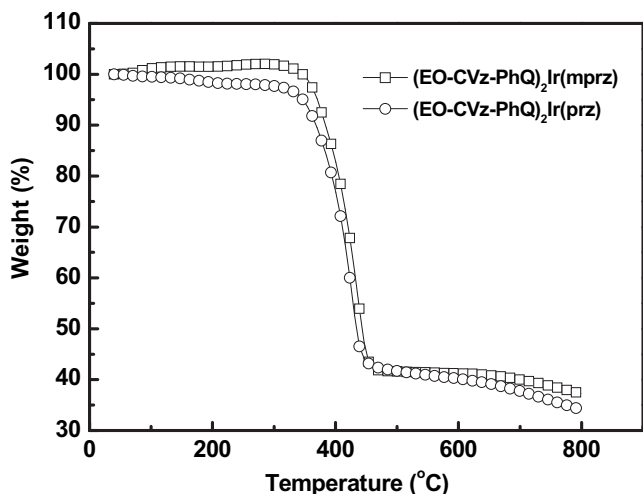


Fig. 1. TGA trace of iridium complexes measured at a scan rate of 10 °C/min under N₂ atmosphere.

5% weight loss) are given in Fig. 1 and summarized in Table 1. The two iridium complexes are thermally stable up to 340 °C, as determined by TGA, which is beneficial to the long-term stability of the PhOLEDs devices fabricated from these materials. From the DSC measurements, we observed distinct glass transition temperatures (T_g) of (EO-CVz-PhQ)₂Ir(prz) and (EO-CVz-PhQ)₂Ir(mprz) at 160 and 164 °C, respectively. To prevent their degradation through the morphological changes of the amorphous organic layer, materials having relatively high T_g values are needed for the fabrication of PhOLEDs [31].

2.3. Photophysical properties

Fig. 2 displays the UV–visible absorption (a) and photoluminescence (PL) (b) spectra of the two iridium complexes dissolved in chloroform solution. The photophysical parameters of the iridium complexes are summarized in Table 1. The main absorption peak at 315 nm, with shoulder peaks at 356 and 410 nm and additional broad tail peaks in the range of 450–550 nm, are observed. In all cases, the higher energy absorption peaks below 400 nm are assigned to the spin-allowed $^1\pi-\pi^*$ transitions of the cyclometalated ligands. The absorption peaks extending into the visible region around 480 nm can be assigned to the spin-allowed metal–ligand charge-transfer band ($^1\text{MLCT}$) and the weak bands at the longer wavelength can be assigned to both spin-orbit coupling enhanced $^3\pi-\pi^*$ and $^3\text{MLCT}$ transition [32]. As a result, the two iridium complexes exhibit very similar $^1\pi-\pi^*$, $^1\text{MLCT}$ and $^3\text{MLCT}$ absorptions, suggesting that the ancillary ligand makes only a small contribution to the absorption process. To investigate the effective overlap between the PL spectrum of the host and the absorption

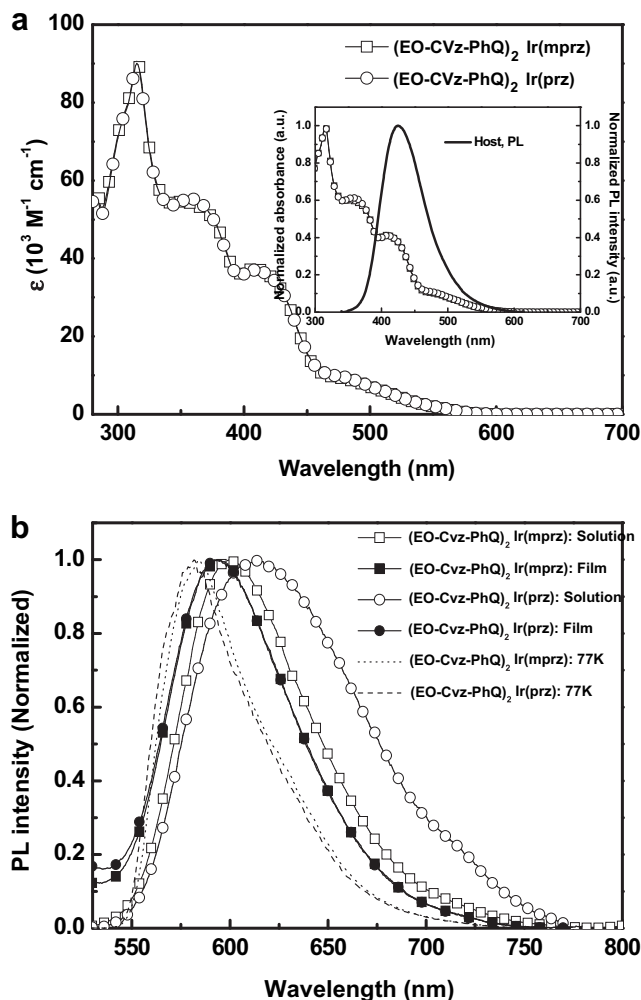


Fig. 2. Absorption (a) and PL (b) spectra of the (EO-CVz-PhQ)₂Ir(prz) and (EO-CVz-PhQ)₂Ir(mprz) in CHCl₃ at 293 K. Inset: Absorption spectra of the (EO-CVz-PhQ)₂Ir(prz) and (EO-CVz-PhQ)₂Ir(mprz) and PL spectrum of host.

spectra of (EO-CVz-PhQ)₂Ir(prz) and (EO-CVz-PhQ)₂Ir(mprz), their spectra were measured, as shown in the inset of Fig. 2(a). This overlap should enable the efficient Förster energy transfer from the singlet-excited state in the host to the MLCT band of the guest, followed by fast intersystem crossing to the triplet state of (EO-CVz-PhQ)₂Ir(prz) and (EO-CVz-PhQ)₂Ir(mprz) and, consequently, emission from their triplet state. The solution state PL spectra of (EO-CVz-PhQ)₂Ir(prz) and (EO-CVz-PhQ)₂Ir(mprz) show the emission of red light with main peaks at 613 and 600 nm, respectively, as shown in Fig. 2(b). The spectra are broad and structureless, implying that the lowest triplet states of these iridium complexes

Table 1
Photophysical, electrochemical and thermal data for synthesized red emitting iridium complexes.

Compound	T_d (°C) ^a	T_g (°C) ^b	λ_{abs} (log ϵ (nm)) ^c	λ_{em} (nm) ^d	λ_{em} (nm) ^e	λ_{em} (nm) ^f	Φ_{pl} (%) ^g	HOMO/LUMO (eV) ^h
(EO-CVz-PhQ) ₂ Ir(mprz)	369	164	315(1.96), 352(1.74), 408(1.57)	600	594	584	0.015	–5.23/–2.70
(EO-CVz-PhQ) ₂ Ir(prz)	346	160	315(1.95), 356(1.74), 410(1.56)	613	593	582	0.006	–5.23/–2.85

^a Temperature with 5% mass loss measure by TGA with a heating rate of 10 °C/min under N₂.

^b Glass transition temperature, determined by DSC with a heating rate of 10 °C/min under N₂.

^c Measured in CHCl₃ solution.

^d Maximum emission wavelength, measured in CHCl₃ solution (298 K).

^e Maximum emission wavelength, measured in PMMA film (298 K).

^f Maximum emission wavelength, measured in CHCl₃ solution (77 K).

^g Measured in 1 × 10^{–5} M degassed CHCl₃ solution relative to Ir(piq)₂(acac) ($\Phi_{\text{pl}} = 0.20$) with 450 nm excitation.

^h Determined from the half-wave potentials for oxidation and reduction.

are likely dominated by the $^3\text{MLCT}$ excited state. On the other hand, the PL spectra of the iridium complexes doped (8 wt%) in poly (methyl methacrylate) (PMMA) films exhibit smaller hypsochromic shifts compared to those in the solution state. The characteristic hypsochromic shift of the PL spectra of the iridium complexes in the film state are thought to be related to the motional relaxation of the excited-state geometry, which is prone to be affected by the rigidity of the matrix. Furthermore, a similar hypsochromic shift was also observed when the CHCl_3 solution of the two iridium complexes was frozen (77 K). The hypsochromic shift observed at 77 K is mainly due to the solvent reorganization in a fluid solution at low temperature that can stabilize the charge-transfer states prior to emission [33]. This process is significantly impeded in a rigid matrix at 77 K and, hence, phosphorescence occurs at a higher energy. We further investigated the photophysical properties of the iridium complexes by measuring their PL quantum yields (Φ_{pl}) in dilute degassed CHCl_3 solutions at 298 K (Table 1).

2.4. Electrochemical properties

To investigate the electrochemical properties of $(\text{EO-CVz-PhQ})_2\text{Ir}(\text{prz})$ and $(\text{EO-CVz-PhQ})_2\text{Ir}(\text{mprz})$, we estimated their highest occupied molecular orbital (HOMO) and lowest unoccupied molecular orbital (LUMO) energy levels by cyclic voltammetry (CV). The CV measurements were carried out in a three electrode cell setup with a 0.1M solution of tetra-*n*-butylammonium hexafluorophosphate (TBAPF₆) in anhydrous acetonitrile/benzene (1:1.5 v/v). The CV curves were referenced to an Ag/AgNO_3 reference electrode, which was calibrated using a ferrocene/ferrocenium (Fc/Fc^+) redox couple (4.8 eV below the vacuum level) as an external standard [34]. The $E_{1/2}$ of the Fc/Fc^+ redox couple was found to be 0.50 V vs. the Ag/AgNO_3 reference electrode. Therefore, the HOMO and LUMO energy levels of $(\text{EO-CVz-PhQ})_2\text{Ir}(\text{prz})$ and $(\text{EO-CVz-PhQ})_2\text{Ir}(\text{mprz})$ can be calculated using the empirical equation $E_{\text{HOMO}} = E_{1/2}(\text{ox}) + 4.30 \text{ eV}$ and $E_{\text{LUMO}} = E_{1/2}(\text{red}) + 4.30 \text{ eV}$, respectively, where $E_{1/2}(\text{ox})$ and $E_{1/2}(\text{red})$ stand for the half-wave potentials for oxidation and reduction relative to the Ag/AgNO_3 reference electrode, respectively. The CV curves of $(\text{EO-CVz-PhQ})_2\text{Ir}(\text{prz})$ and $(\text{EO-CVz-PhQ})_2\text{Ir}(\text{mprz})$ are shown in Fig. 3. In all of the cases, the electrochemical switching was reversible and the CV curves remained unchanged under multiple successive potential scans, suggesting their excellent stability against electrochemical oxidation and reduction. On the basis of the oxidation and reduction potentials, $(\text{EO-CVz-PhQ})_2\text{Ir}(\text{prz})$ and $(\text{EO-CVz-PhQ})_2\text{Ir}(\text{mprz})$ exhibited in the ranges of 0.93 V and -1.45 to -1.60 V, respectively. From the results, the HOMO and LUMO energy levels of $(\text{EO-CVz-PhQ})_2\text{Ir}(\text{prz})$ and $(\text{EO-CVz-PhQ})_2\text{Ir}(\text{mprz})$ were calculated to be -5.23 eV and -2.85 to -2.70 eV , respectively. The HOMO and LUMO energy levels are summarized in Table 1.

2.5. Electroluminescence properties

We evaluated the potential of $(\text{EO-CVz-PhQ})_2\text{Ir}(\text{prz})$ and $(\text{EO-CVz-PhQ})_2\text{Ir}(\text{mprz})$ as red emissive materials in PhOLEDs applications with the configuration of ITO/PEDOT:PSS/TCTA (30 nm)/EML (50 nm)/OXD-7 (20 nm)/Ba (3 nm)/Al (100 nm). As a host, we selected a blend of poly(vinylcarbazole) (PVK), *N,N'*-diphenyl-*N,N'*-(bis(3-methylphenyl)-[1,1-biphenyl]-4,4'-diamine) (TPD) as the hole transport material and 1,3-bis[5-(4-*tert*-butylphenyl)-1,3,4-oxadiazole-2-yl]benzene (OXD-7) as the electron transport material. Fig. 4 displays the relative HOMO and LUMO energy levels of the materials used to fabricate the PhOLEDs. The energy level diagrams show that the energy levels of $(\text{EO-CVz-PhQ})_2\text{Ir}(\text{prz})$ and $(\text{EO-CVz-PhQ})_2\text{Ir}(\text{mprz})$ (both HOMO and LUMO) lie above and below those of the host, respectively. Consequently, it is possible that iridium

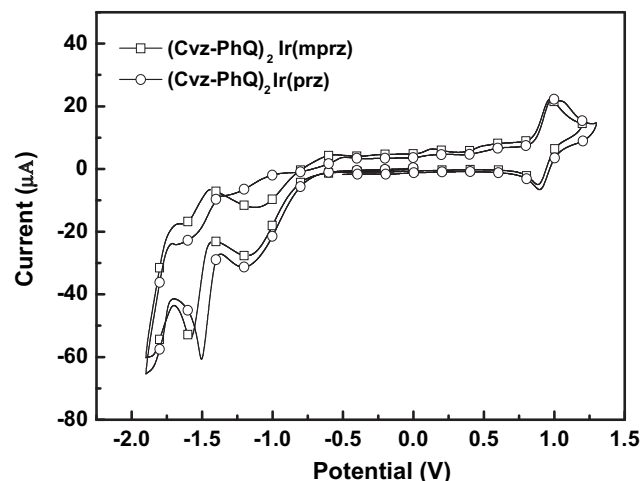


Fig. 3. Cyclic voltammograms of iridium complexes in tetra-*n*-butylammonium hexafluorophosphate (TBAPF₆) at a scan rate of 100 mV/s.

complexes would be able to trap both electrons and holes in the emitting layer. Moreover, a hole blocking or electron transport (OXD-7) layer was introduced for effective electron injection/facilitate and charge carrier balance within the emitting layer. The LUMO energy level of OXD-7 is closely aligned to the LUMO energy level of the iridium complexes in the emitting layer.

Fig. 4 displays the relative HOMO and LUMO energy levels of the materials used to fabricate the PhOLEDs. The energy level diagrams show that the energy levels of $(\text{EO-CVz-PhQ})_2\text{Ir}(\text{prz})$ and $(\text{EO-CVz-PhQ})_2\text{Ir}(\text{mprz})$ (both HOMO and LUMO) lie above and below those of the host, respectively. Consequently, it is possible that iridium complexes would be able to trap both electrons and holes in the emitting layer. Moreover, a hole blocking or electron transport (OXD-7) layer was introduced for effective electron injection/facilitate and charge carrier balance within the emitting layer. The LUMO energy level of OXD-7 is closely aligned to the LUMO energy level of the iridium complexes in the emitting layer.

Fig. 5 displays the electroluminescent (EL) spectra of $(\text{EO-CVz-PhQ})_2\text{Ir}(\text{prz})$ and $(\text{EO-CVz-PhQ})_2\text{Ir}(\text{mprz})$ at a current density of 10 mA/cm² and their PL film spectra. The EL spectra exhibited a red emission with a peak maximum at 600 nm and excellent color purity at a CIE coordinate of (0.60, 0.39). The PL film spectra of $(\text{EO-CVz-PhQ})_2\text{Ir}(\text{prz})$ and $(\text{EO-CVz-PhQ})_2\text{Ir}(\text{mprz})$ showed a slight difference from their EL spectra, corresponding to a red-shift of

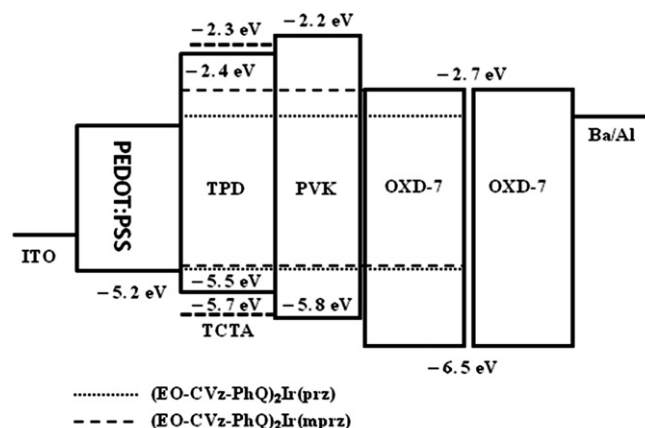


Fig. 4. The relative HOMO/LUMO energy levels of the materials used for the PhOLEDs.

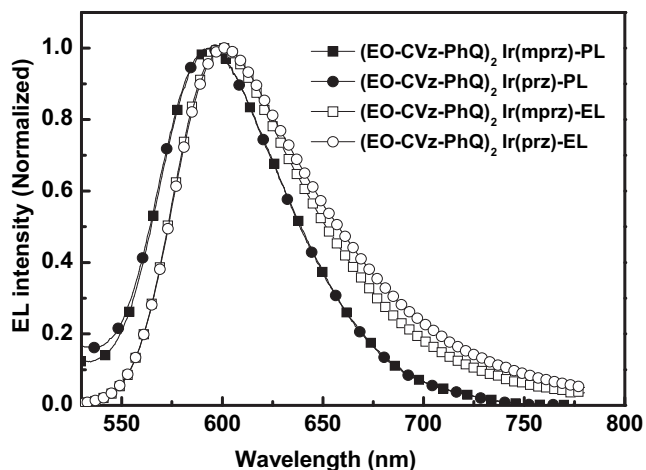


Fig. 5. EL and PL spectra (film state) of (EO-CVz-PhQ)₂Ir(prz) and (EO-CVz-PhQ)₂Ir(mprz).

about 5 nm. These differences between the EL and PL spectra are attributed to the optical effect caused by the recombination zone shift [35].

Fig. 6(a) displays the current density-voltage-luminance (*J-V-L*) characteristics of these red PhOLEDs. The maximum luminances of the PhOLEDs using (EO-CVz-PhQ)₂Ir(prz) and (EO-CVz-PhQ)₂Ir(mprz) were found to be 4024 and 7219 cd/m² and their turn-on voltages were 5.6 and 5.6 V, respectively. The PhOLEDs with the (EO-CVz-PhQ)₂Ir(mprz) dopant exhibited a higher current density than that of those with the (EO-CVz-PhQ)₂Ir(prz) dopant at the same voltage. This result can be explained by the efficient electron injection or transport from the Al cathode to the emitting layer. (EO-CVz-PhQ)₂Ir(prz) and (EO-CVz-PhQ)₂Ir(mprz) have LUMO energy levels of −2.85 and −2.70 eV, respectively. As can be seen in Fig. 4, electrons are somewhat trapped by (EO-CVz-PhQ)₂Ir(prz), due to the LUMO gap of 0.15 eV between OXD-7 and (EO-CVz-PhQ)₂Ir(prz). On the other hand, the LUMO gap between OXD-7 and (EO-CVz-PhQ)₂Ir(mprz) is 0 eV, which is very well aligned with the LUMO energy level of (EO-CVz-PhQ)₂Ir(mprz). Fig. 6(b) displays the luminance efficiency and power efficiency versus the current density characteristics and the performances of the red PhOLEDs are summarized in Table 2. The maximum luminance efficiencies of

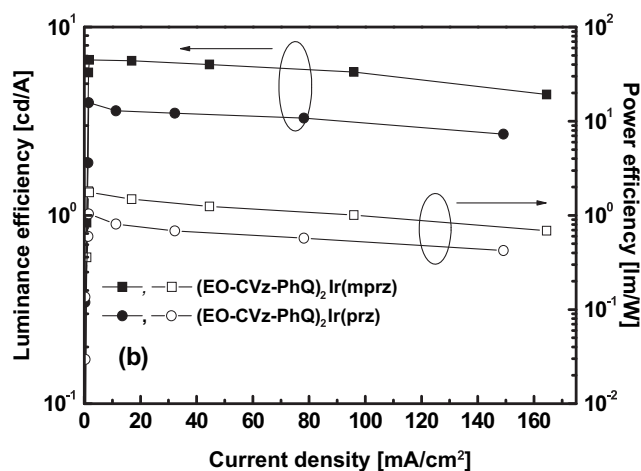


Fig. 6. Current density-voltage-luminance (a) and luminance and power efficiency-current density (b) characteristics of (EO-CVz-PhQ)₂Ir(prz) and (EO-CVz-PhQ)₂Ir(mprz).

Table 2

EL performance of red PhOLED based on a solution processed emitting layer.

Emitter	Turn-on (V) ^a	<i>L</i> _{max} (cd/m ²)	EQE _{max} (%)	LE _{max} (cd/A)	PE _{max} (lm/W)	CIE (x, y) ^b
(EO-CVz-PhQ) ₂ Ir(mprz)	5.6	7219	3.68	6.69	1.80	0.60, 0.39
(EO-CVz-PhQ) ₂ Ir(prz)	5.6	4024	2.33	3.96	1.03	0.60, 0.39

^a Luminance is 1 cd/m².

^b Recorded at current density 10 mA/cm².

the PhOLEDs using (EO-CVz-PhQ)₂Ir(prz) and (EO-CVz-PhQ)₂Ir(mprz) were found to be 3.96 and 6.69 cd/A and their maximum power efficiencies were 1.03 and 1.80 lm/W, respectively. When using (EO-CVz-PhQ)₂Ir(mprz) as an emitter, the PhOLEDs exhibited an efficiency of 6.69 cd/A at a low current density of 1.81 mA/cm². On the other hand, at a high current density of 44.59 mA/cm², the PhOLEDs exhibited a luminance efficiency of 6.33 cd/A, with only a 5.4% luminance efficiency roll-off being observed. From this result, it can be concluded that the problematic efficiency roll-off in PhOLEDs can also be suppressed by introducing a TCTA interlayer between the emitting layer and PEDOT:PSS. This phenomenon may be explained by the fact that the TCTA interlayer renders the carrier injection to the PVK host more efficient and blocks the electrons at the TCTA/EML interface, thus allowing them to be better confined at the interface. The roll-off of the PhOLEDs using (EO-CVz-PhQ)₂Ir(prz) as an emitter showed a similar trend to that of the PhOLEDs based on (EO-CVz-PhQ)₂Ir(mprz).

3. Conclusion

We successfully synthesized a new iridium complexes with a carbazole containing phenylquinoline (CVz-PhQ) derivative, in order to fabricate solution processed, red PhOLEDs. The fabricated red PhOLEDs with the configuration of ITO/PEDOT:PSS/TCTA interlayer/PVK:TPD:OXD-7:iridium complex/cathode exhibited maximum external quantum and luminance efficiency values of 3.68% and 6.69 cd/A, respectively. Furthermore, by introducing a TCTA interlayer between the emitting layer and PEDOT:PSS, the efficiency roll off can be suppressed through effective carrier injection and electron blocking within the emitting layer.

4. Experimental

4.1. Characterization

¹H NMR and ¹³C NMR spectra were recorded on a Varian Mercury Plus 300 MHz spectrometer and the chemical shifts were recorded in ppm units with CDCl₃ as the internal standard. The thermal analyses were carried out on a Mettler Toledo TGA/SDTA 851^e, DSC 822^e analyzer under an N₂ atmosphere at a heating rate of 10 °C/min. CV was carried out with a CHI 600C potentiostat (CH Instruments) at a scan rate of 100 mV/s in a 0.1 M solution of tetra-*n*-butylammonium hexafluorophosphate (TBAPF₆) in anhydrous acetonitrile/benzene (1:1.5 v/v). A platinum wire was used as the counter electrode and an Ag/AgNO₃ electrode was used as the reference electrode. UV-visible spectra were measured using a JASCO V-570 spectrophotometer. PL spectra and low-temperature phosphorescence spectra were obtained using Hitachi F-4500 fluorescence spectrophotometer.

4.2. Synthesis of (EO-CVz-PhQ)₂Ir(prz) or (EO-CVz-PhQ)₂Ir(mprz)

9-(2-(2-Methoxy-ethoxy)ethyl)-3-(4-phenylquinolin-2-yl)-9H-carbazole (EO-CVz-PhQ) (1.07 g, 2.27 mmol) and IrCl₃·H₂O (0.32 g, 0.91 mmol) were added to a mixture of 2-ethoxyethanol and water

(80 mL, 3:1 v/v). The reaction mixture was stirred at 140 °C for 20 h and a brown precipitate was obtained after cooling at room temperature. The precipitate was collected and washed with deionized water (80 mL) and methanol (40 mL). Subsequently, the cyclometalated iridium dimer was dried under vacuum to afford a brown solid. Cyclometalated iridium dimer (0.6 g, 0.26 mmol) and 2-pyrazinecarboxylic acid (0.16 g, 1.28 mmol) or 5-methyl-2-pyrazinecarboxylic acid (0.18 g, 1.28 mmol) were mixed with Na₂CO₃ (0.27 g, 2.56 mmol) in 2-ethoxyethanol (30 mL). The mixture was refluxed for 12 h under a N₂ atmosphere. After cooling at room temperature, the crude solution was poured onto water and extracted with ethyl acetate, dried over anhydrous MgSO₄ and evaporated in a vacuum. The residue was purified by silica gel chromatography (hexane:ethyl acetate = 1:4) as an eluent and further purified by recrystallization twice using dichloromethane/hexane mixture to afford a red solid complex (0.25 g, 78%).

4.2.1. (EO-CVz-PhQ)₂Ir(prz)

¹H NMR (300 MHz, CDCl₃): δ (ppm): 9.04 (s, 1H), 8.78 (d, 2H), 8.64 (s, 1H), 8.55 (s, 1H), 8.27 (s, 1H), 8.13 (d, *J* = 7.8 Hz, 1H), 8.04 (d, 1H), 7.82–7.61 (m, 12H), 7.51–7.12 (m, 12H), 7.03 (s, 1H), 6.86 (t, 1H), 6.32 (s, 1H), 4.09–3.77 (m, 4H), 3.58–3.25 (m, 4H), 3.15–2.88 (m, 14H) ¹³C NMR (300 MHz, CDCl₃): δ (ppm): 170.8, 170.2, 168.5, 150.6, 150.5, 148.6, 147.9, 147.1, 147.0, 146.6, 144.0, 142.8, 142.2, 140.4, 140.3, 139.2, 138.5, 137.6, 137.5, 137.3, 129.5, 129.1, 129.0, 128.8, 128.7, 126.4, 126.1, 125.5, 125.2, 125.1, 125.0, 124.6, 123.9, 123.8, 119.7, 119.3, 119.1, 119.0, 118.9, 118.0, 117.0, 115.2, 113.6, 109.0, 108.7, 71.6, 71.3, 70.2, 70.1, 68.0, 67.5, 59.0, 58.9, 41.9. Anal. Calcd. For C₆₉H₅₇N₆O₆Ir: C, 65.85; H, 4.57; N, 6.68; found: C, 66.15; H, 4.63; N, 6.56.

4.2.2. (EO-CVz-PhQ)₂Ir(mprz)

¹H NMR (300 MHz, CDCl₃): δ (ppm): 8.92 (s, 1H), 8.81–8.77 (t, 2H), 8.63 (s, 1H), 8.27 (d, *J* = 7.8 Hz, 1H), 8.14 (d, *J* = 7.2 Hz, 1H), 8.04 (d, *J* = 7.8 Hz, 1H), 7.85–7.58 (m, 12H), 7.54–7.12 (m, 12H), 7.00 (s, 1H), 6.85 (t, 1H), 6.30 (s, 1H), 4.07–3.73 (m, 4H), 3.58–3.43 (m, 4H), 3.32–2.86 (m, 14H), 2.47 (s, 3H) ¹³C NMR (300 MHz, CDCl₃): δ (ppm): 170.8, 170.3, 168.6, 158.4, 150.6, 150.5, 148.6, 147.8, 147.0, 146.8, 144.1, 142.8, 142.2, 140.4, 140.3, 139.2, 138.5, 137.6, 137.5, 137.4, 129.7, 129.2, 129.0, 128.8, 128.7, 126.4, 126.1, 125.6, 125.2, 125.1, 125.0, 124.7, 123.9, 123.8, 119.7, 119.4, 119.1, 119.0, 118.9, 118.0, 117.0, 115.2, 113.6, 109.0, 108.7, 71.6, 71.5, 70.2, 70.1, 68.1, 67.7, 59.0, 58.9, 42.0, 22.1. Anal. Calcd. For C₇₀H₅₉N₆O₆Ir: C, 66.07; H, 4.67; N, 6.60; found: C, 66.16; H, 4.64; N, 6.54.

4.3. Fabrication of PhOLEDs and measurement

The PhOLEDs were fabricated in the configuration ITO/PEDOT:PSS (40 nm)/TCTA (30 nm)/doped emitting layer (50 nm)/OXD-7 (20 nm)/Ba (3 nm)/Al (100 nm). The indium tin oxide (ITO) glass substrates with a sheet resistance of 20 Ω per square was washed in turn with a substrate-cleaning detergent, deionized water, acetone, and isopropyl alcohol, and finally treated with UV–ozone chamber for 20 min. The PEDOT:PSS (40 nm, CLEVIOS P VP Al 4083) was spin-coated directly onto the patterned ITO glass and baked in air at 150 °C for 10 min. Subsequently, the TCTA interlayer solution (0.5 wt% in toluene) was spin coated and then dried at 180 °C for 30 min on a hot plate. The emitting layer was then spin-coated onto the interlayer coated substrate from a mixed solution of PVK, TPD, OXD-7 (weight ratio, 2:1:1), and doped with 8 wt% of (EO-CVz-PhQ)₂Ir(prz) or (EO-CVz-PhQ)₂Ir(mprz). All solutions used in the PhOLEDs fabrication were filtered with 0.20 μm PTFE syringe filter. The emitting layer was then baked at 80 °C for 30 min in glove box. Finally, as typical cathode, consisting of OXD-7 (20 nm)/Ba (3 nm)/Al (100 nm) was thermal vapor

deposited with effective area of 4 mm² at a pressure 5 × 10⁻⁶ Torr. The film thickness was measured by using α-Step IQ surface profiler (KLA Tencor, San Jose, CA). EL spectra and current density-voltage-luminance (*J-V-L*) characteristics of PhOLEDs were measured with a programmable Keithley model 236 power source and spectrascan CS-1000 photometer, respectively. All measurements were carried out at room temperature under an ambient atmosphere without encapsulation.

Acknowledgements

This work was supported by National Research Foundation of Korea (NRF) grant funded from the Ministry of Education, Science and Technology (MEST) of Korea (No. M10600000157-06J0000-15710) and Basic Science Research Program through the National Research Foundation of Korea (NRF) grant funded from the Ministry of Education, Science and Technology (MEST) of Korea for the Center for Next Generation Dye-sensitized Solar Cells (No. 2010-0001842). This work was supported by the New & Renewable Energy program of the Korea Institute of Energy Technology Evaluation and Planning (KETEP) grant (No. 20103020010050) funded by the Ministry of Knowledge Economy, Republic of Korea.

References

- [1] M.A. Baldo, D.F. O'Brien, Y. You, A. Shoustikov, S. Sibley, M.E. Thompson, S.R. Forrest, *Nature* 395 (1998) 151–154.
- [2] S. Lamansky, P. Djurovich, D. Murphy, F. Adbel-Razzaq, H.E. Lee, C. Adachi, P.E. Burrows, S.R. Forrest, M.E. Thompson, *J. Am. Chem. Soc.* 123 (2001) 4304–4312.
- [3] A. Tsuboyama, H. Iwakaki, M. Furugori, T. Mukaide, J. Kamatani, S. Igawa, T. Moriyama, S. Miura, T. Takiguchi, S. Okada, M. Hoshino, K. Ueno, *J. Am. Chem. Soc.* 125 (2003) 12971–12979.
- [4] R.N. Bera, N. Cumpstey, P.L. Burn, I.D.W. Samuel, *Adv. Funct. Mater.* 17 (2007) 1149–1152.
- [5] S.C. Lo, N.A.H. Male, J.P.J. Markham, S.W. Magennis, P.L. Burn, O.V. Salata, I.D.W. Samuel, *Adv. Mater.* 14 (2002) 975–979.
- [6] C.L. Lee, K.B. Lee, J.J. Kim, *Appl. Phys. Lett.* 77 (2000) 2280–2282.
- [7] X. Gong, M.R. Robinson, K.C. Ostrowski, D. Moses, G.C. Bazan, A.J. Heeger, *Adv. Mater.* 14 (2002) 581–585.
- [8] J.C. Ostrowski, M.R. Robinson, A.J. Heeger, G.C. Bazan, *Chem. Commun.* (2002) 784–785.
- [9] X.H. Yang, F.I. Wu, D. Neher, C.H. Chien, C.F. Shu, *Chem. Mater.* 20 (2008) 1629–1635.
- [10] Y.J. Pu, M. Higashidate, K.I. Nakayama, J. Kido, *J. Mater. Chem.* 18 (2008) 4183–4188.
- [11] S.C. Lo, G.J. Richards, J.P.I. Markham, E.B. Namdas, S. Sharma, P.L. Burn, I.D.W. Samuel, *Adv. Funct. Mater.* 15 (2005) 1451–1458.
- [12] I.A. Barlow, T. Kreouzis, D.G. Lidzey, *Appl. Phys. Lett.* 94 (2009) 243301–243303.
- [13] D. Krautz, E. Lunedei, J. Puigdollers, G. Badenes, R. Alcubilla, S. Cheylan, *Appl. Phys. Lett.* 96 (2010) 033301–033303.
- [14] M.J. Harding, D. Poplavskyy, V.E. Choong, F. So, A.J. Campbell, *Adv. Funct. Mater.* 20 (2010) 119–130.
- [15] J. Ding, J. Lü, Y. Cheng, Z. Xie, L. Wang, X. Jing, F. Wang, *Adv. Funct. Mater.* 18 (2008) 2754–2762.
- [16] B. Liang, L. Wang, Y. Xu, H. Shi, Y. Cao, *Adv. Funct. Mater.* 17 (2007) 3580–3589.
- [17] G. Zhou, W.Y. Wong, B. Yao, Z. Xie, L. Wang, *Angew. Chem. Int. Ed. Engl.* 46 (2007) 1149–1151.
- [18] A.W. Freeman, S.C. Koene, P.R.L. Malenfant, M.E. Thompson, J.M.J. Fréchet, *J. Am. Chem. Soc.* 122 (2000) 12385–12386.
- [19] S.C. Lo, R.E. Harding, C.P. Shipley, S.G. Stevenson, P.L. Burn, I.D.W. Samuel, *J. Am. Chem. Soc.* 131 (2009) 16681–16688.
- [20] W.S. Huang, C.W. Lin, J.T. Lin, J.H. Huang, C.W. Chu, Y.H. Wud, H.C. Lin, *Org. Electron* 10 (2009) 594–606.
- [21] H. Zhen, C. Luo, W. Yang, W. Song, B. Du, J. Jiang, C. Jiang, Y. Zhang, Y. Cao, *Macromolecules* 39 (2006) 1693–1700.
- [22] S. Tokito, M. Suzuki, F. Sato, M. Kamachi, K. Shirane, *Org. Electron* 4 (2003) 105–111.
- [23] X. Chen, J.L. Liao, Y. Liang, M.O. Ahmed, H.E. Tseng, S.-A. Chen, *J. Am. Chem. Soc.* 125 (2003) 636–637.
- [24] Lei Wang, Yang Jiang, Jia Luo, Yan Zhou, Junhong Zhou, Jian Wang, Jian Pei, Yong Cao, *Adv. Mater.* 21 (2009) 4854–4858.
- [25] J. Huang, T. Watanabe, K. Ueno, Y. Yang, *Adv. Mater.* 19 (2007) 739–743.
- [26] S.O. Jung, Q. Zhao, J.W. Park, S.O. Kim, Y.H. Kim, H.Y. Oh, J. Kim, S.K. Kwon, Y. Kang, *Org. Electron* 10 (2009) 1066–1073.

- [27] R.J. Holmes, S.R. Forrest, Y.J. Tung, R.C. Kwong, J.J. Brown, S. Garon, M.E. Thompson, *Appl. Phys. Lett.* 82 (2003) 2422–2424.
- [28] C. Yang, X. Zhang, H. You, L. Zhu, L. Chen, L. Zhu, Y. Tao, D. Ma, Z. Shuai, J. Qin, *Adv. Funct. Mater.* 17 (2007) 651–661.
- [29] S.J. Lee, J.S. Park, M. Song, I.A. Shin, Y.I. Kim, J.W. Lee, J.W. Kang, Y.S. Gal, S. Kang, J.Y. Lee, S.H. Jung, H.S. Kim, M.Y. Chae, S.H. Jin, *Adv. Funct. Mater.* 19 (2009) 2205–2212.
- [30] M. Nonoyama, *J. Organomet. Chem.* 86 (1975) 263–267.
- [31] Masaru Nagai, Hisakazu Nozoye, *J. Electrochem. Soc.* 154 (2007) J239–J245.
- [32] H.H. Rho, G.Y. Park, Y. Ha, Y.S. Kim, *Jpn. J. Appl. Phys.* 45 (2006) 568–573.
- [33] A.B. Tamayo, S. Garon, T. Sajoto, P.I. Djurovich, I.M. Tsyba, R. Bau, M.E. Thompson, *Inorg. Chem.* 44 (2005) 8723–8732.
- [34] H.J. Cho, B.J. Jung, N.S. Cho, J. Lee, H.K. Shim, *Macromolecules* 36 (2003) 6704–6710.
- [35] S.O. Jeon, K.S. Yook, C.W. Joo, J.Y. Lee, *Appl. Phys. Lett.* 94 (2009) 013301–013303.